Guest-Anion-Induced Rotation-Restricted Emission in UiO-66-NH_2 and Advanced Structure Elucidation

Qi Xue[a,b †], Ka Hin Chan[a,b †], Cheuk Ki Yim[b], Bryan Kit Yue Ng[c], Tianxiang Chen[b], Sarah Day[d], Chiu Chung Tang[d], Shogo Kawaguchi[e], Kwok Yin Wong[b], Tsz Woon Benedict Lo[a,b]*

[a.] The Hong Kong Polytechnic University Shenzhen Research Institute, Shenzhen, 519700, China

[b.] State Key Laboratory of Chemical Biology and Drug Discovery, Department of Applied Biology and Chemical Technology, The Hong Kong Polytechnic University, Hong Kong, China

[c.] Department of Chemistry, University of Oxford, Oxford, OX1 3QR, United Kingdom

[d.] Diamond Light Source, Harwell Campus, Didcot, OX11 0DE, United Kingdom

[e.] SPring-8, Hyogo, 679-5198, Japan

[†] These authors contributed equally to this work as joint first authors.

KEYWORDS. Photoluminescence enhancement, rotation-restricted emission, metal-organic frameworks, Rietveld refinement, anion sensing.

ABSTRACT: We report the guest-anion-induced photoluminescence enhancement of metal-organic frameworks (UiO-66-NH_2), firstly based upon diffraction and computational evidence. We found that only limited anions, namely carbonate and fluoride, can lead to a significant enhancement in photoluminescence whereas their related anions, such as acetate and chloride, cannot. The optimized crystal structures reveal that the guest carbonate and fluoride ions interact with four framework amino-functional groups through hydrogen bonding (*ca.* 1.6-1.7 Å) that ultimately forms a quaternary (-N(H))$_4$…X^- molecular bridge around the nodal center. Hence, the hydrogen-bonded molecular bridge not only restricts the intermolecular C-C rotation of the linker molecules, but also greatly perturbs the electronic densities between the guest anions and the framework amino groups.

Introduction

Metal-organic frameworks (MOFs) are a relatively new class of micro/mesoporous solid-state materials constructed by the reticular assembly of numerous periodically connected metal/metal-cluster nodal centers and multifunctional linker molecules. Interesting optical properties have been reported in different MOFs.[1,2] Researchers have widely utilized the luminescent properties of MOFs in various applications, such as gas sensing, anion/cation detection, amino acid sensing, and temperature probing.[3] The intrinsic luminescent property of a typical MOF originates from charge transfer transitions between the atomic/molecular moieties, such as metal-to-ligand charge transfer, ligand-to-metal charge transfer, and ligand-to-cluster charge transfer. The luminescent property can be altered by incorporating guest species, leading to extensive sensing applications. Notably, by post-synthetic modification, lanthanide ions (such as Eu^{2+} and Tb^{3+}) can be incorporated into the MOF structures.[4,5] Lanthanide ions are inherently luminescent due to *f-f* transition, resulting in highly long-lived excited states. The organic linkers can hereby act as an 'antenna' to amplify the luminescent signal. Incorporating other guest molecules/ions can also affect the luminescent property, for instance, the addition of Fe^{3+} that can quench the fluorescence of UiO-66-NH_2[6], *etc.*[7–11] Thonhauser *et al.* recently discussed the guest-induced structural change in a Zn-based MOF based on theoretical findings, which is the primary reason causing the 'turn-on' PL enhancement.[12] Besides the guest-induced effect, external factors, such as temperature[13], pressure[14], and solvent polarity[15], can also alter the fluorescence property. Moggach *et al.* recently reported the linker molecules (1,4-phenylene-bis(4-ethynylbenzoate)) in a Hf-based MOF that can rotate from a coplanar to a twisted arrangement as induced by external pressure[14], whereas Tsang *et al.* have reported the ammonia induced intramolecular linker rotation in a UiO-67-derivative[16]. The change in the linker conformation leads to bathochromic shifts in both fluorescence emission and ultra-violet/visible light absorption spectra.

Indeed, many atomic-scale processes can modify the fluorescence property in MOFs, which includes antenna effect[17], rotation-restricted emission (RRE)[17], exact guest–host interaction[18], electron charge transfer[19], ionic vibrations[12], *etc.*[10,12,20–25] Among them, RRE is an interesting factor that can extend the lifetime of electrons in the excited states when the intramolecular rotation of molecules is hindered.[25] Although progress has been made to utilize this interesting optical phenomenon particularly for sensing, the fundamental reason for the alternation of luminescence still remains vague. As RRE is highly related to the structural chemistry between the molecular analytes and the MOF frameworks, a systematic structural study can provide realizable findings to unveil the mysteries.

Thanks to the ultra-high crystallinity of many MOFs, the crystallographic and atomic information of the encapsulated extra-framework species (with long-range order) can be revealed with high reliability using scattering- and diffraction-based methods. For instance, Xu *et al.* have reported the cap-

ture of Hg^{2+} and Pd^{2+} in thiol-functionalized UiO-derivatives and studied the adsorption chemistry using single-crystal X-ray diffraction.[26,27] However, growing single crystals of many MOFs can be challenging because of various inherent structural problems, such as pseudosymmetry, intergrowth, and disordered structures.[28] Our group has recently developed a reliable methodology to elucidate the adsorbate structures of small organic molecules (such as ammonia and methanol) within microporous materials.[29,30] The slight-but-subtle alternation in the scattering factors (F_{hkl}) upon the incorporation of adsorbed guest species with long-range order in the MOF structures can greatly affect the intensity of Bragg's reflections.[31] In this work, we utilize the unique chemical and structural functionalities of UiO-66-NH_2 to investigate how specific guest anions, namely CO_3^{2-} and F^-, can enhance the PL signals. The combined Rietveld refinement and first-principle calculation results infer specific binding modes that restrict linker rotation in UiO-66-NH_2 by forming quaternary $(\text{-N(H)})_4\ldots X^-$ molecular bridges *via* hydrogen bonding. This work reveals the tertiary structures of MOF with guest anions, which effectively restricts the rotational order of the linker species. A rational structure-function relation between the adsorbate structures and optical properties is consequently established from an atomistic perspective.

Results and Discussion

A highly crystalline UiO-66-NH_2 powder sample has been prepared and characterized (see Figures S1-S5 in Supporting Information). As determined by synchrotron X-ray powder diffraction, the sample has a space group of *Fm-3m* and the lattice parameter of a = 20.78902(45) Å. Based on the method reported by Lamberti *et al.*, the extent of ligand defect in MOFs can be estimated by thermogravimetric analysis.[38] Hence, the structural formula is calculated to be $Zr_6O_4(OH)_4(ATA)_{5.8}$ (ATA = 2-aminoterephthalic acid; Zr:ATA = 1:0.96), and the sample is almost perfectly crystalline.

The PL spectra of UiO-66-NH_2 with the addition of different anions are presented in Figure 1(a). Note that the PL of pristine UiO-66-NH_2 can be ascribed to the n→π* ligand-to-cluster charge transfer from the lone pair of the amino group on the linker to the Zr_6O_4 nodal center (see Figure S6).[39] Excitingly, we discovered that CO_3^{2-} can increase the PL signal by 1210%. The addition of F^- to UiO-66-NH_2 increases the PL intensity by 444%, consistent with a related finding by Zhu *et al.*[7] It is important to note that the PL enhancement effect is only observed when CO_3^{2-} and F^- are applied (see Figure S7), but the addition of their related anions (CH_3COO^- and Cl^-) does not affect the PL signal. From our binding comparative study, UiO-66-NH_2 can selectively uptake CO_3^{2-} from a mixture of (CO_3^{2-} and CH_3COO^-) and F^- from a mixture of (F^- and Cl^-) as the PL increments match with the addition of a single anion (CO_3^{2-} or F^-). It agrees with previous studies that UiO-66-NH_2 can selectively uptake F^- from a halide mixture that contains F^-, Cl^- and Br^-,[40] due to the strong interactions between F^- and the binding sites in the UiO-66 channels based on molecular dynamics simulation.[41] This can be attributed to the low activation energy for adsorption for F^- by UiO-66-NH_2 and a relatively strong surface physisorption binding.[40] In our control experiments using UiO-66 (see Figure 1(b)), the PL signal is unchanged upon the addition of these anions. Figure S8 shows that the substitution effect by the linker without the amino group substituent, i.e., by replacing ATA with terephthalic acid. It is found that the PL enhancement upon the addition of CO_3^{2-} falls in a linear function with the concentration of ATA linkers.

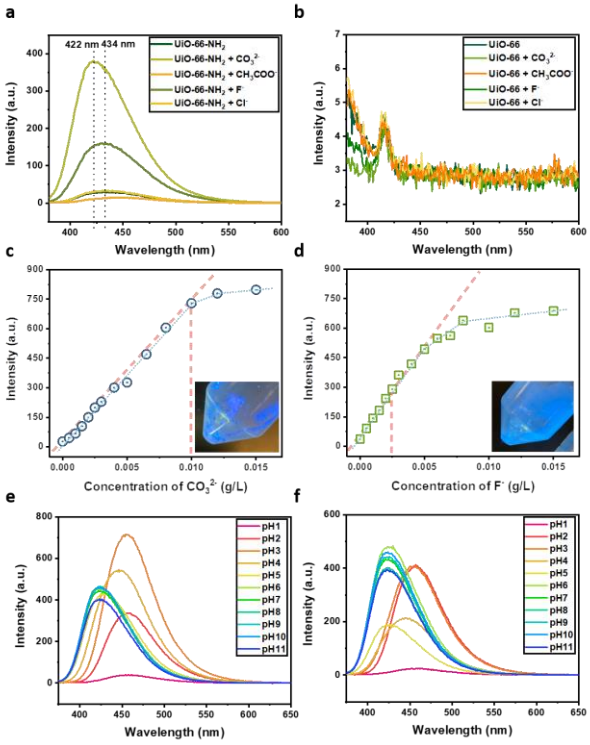

Figure 1. Photoluminescence intensities of (a) UiO-66-NH_2 and (b) UiO-66, with the addition of CO_3^{2-}, CH_3COO^-, F^-, and Cl^- anions. Plotting PL of UiO-66-NH_2 as a function of the concentrations of (c) CO_3^{2-} and (d) F^-. Plotting PL of UiO-66-NH_2 upon adding (e) CO_3^{2-} and (f) F^- as a function of pH values.

We have subsequently studied the concentration dependence of CO_3^{2-} and F^- with respect to UiO-66-NH_2. As presented in Figure 1(c) and (d), the increments of the PL signal are linear at low CO_3^{2-} and F^- concentrations. The linear plots can be extrapolated to the limit of detection.[42] The limits of detection of CO_3^{2-} and F^- were determined as 0.63 mg L^{-1} and 0.12 mg L^{-1}, respectively (see Figure S9). According to the guidelines of the World Health Organization, the level of F^- in drinking water should not exceed 1.5 mg L^{-1}.[43] The CO_3^{2-} in typical drinking water however range between 10 to 100 mg L^{-1}, inferring that UiO-66-NH_2 may not be an appropriate F^- sensor for drinking water due to the interference by CO_3^{2-}. The anion-concentration linearities were discontinued after the stoichiometric ratios of CO_3^{2-} and F^- to the ATA linker, inferring stoichiometric bindings.

To investigate the binding preference of the anions in UiO-66-NH_2 (direct or indirect binding with the framework), the PL properties have been compared with UiO-66-NH_2 modified with 3*d* transition metal ions. 3*d* metal ions, such as Cu^{2+}, can be grafted onto the Lewis basic linker -NH_2 moieties to form acid-base adducts by simple chemical exchange. We have therefore selected Cu^{2+}-modified UiO-66-NH_2 ('Cu^{2+}-UiO-66-NH_2') as a model to verify our postulations, where we have extensively characterized the crystal structure of Cu^{2+}-UiO-66-NH_2 in our recent work, see Figures S10-S11 for the diffrac-

tion and spectroscopic evidence.[44] According to elemental analysis, the Cu-incorporated sample contains 0.10 Cu per Zr, which approximately equals 0.10 Cu per -NH_2. As shown in Figure S12, the PL signal increases by *ca*. 60% upon incorporating Cu^{2+} due to the potential extended charge transfer pathway. As the Cu^{2+} species are simply grafted onto the -NH_2 group through Lewis acid-base interaction, the enhancement in PL signal can be ascribed as a general 'antenna effect'. By loading the Cu^{2+}-UiO-66-NH_2 sample with different anions, the PL signals display percentage changes in perfect agreement with UiO-66-NH_2 (see Figure S13). For the samples with CO_3^{2-} and F^-, the PL intensity increases noticeably, akin to those of UiO-66-NH_2 that increase by 460% and 1080%, respectively. Likewise, the PL signals stay unchanged upon the addition of Cl^- and CH_3COO^-. Thus, it can be concluded that the grafted Cu^{2+} plays no active role for PL enhancement besides a sheer antenna effect. This experiment has offered solid evidence on the direct binding preference of the anions with the parent MOF structure.

Since the Zr_6O_4 nodes and amino groups on UiO-66-NH_2 are sensitive to pH, we employed a set of pH-dependent experiments to investigate the selective bindings of CO_3^{2-} and F^- by UiO-66-NH_2. As seen in Figure 1(e) and (f), the PL intensities of UiO-66-NH_2 with CO_3^{2-} and F^- at different pH values (pH 1-11) show a clear pattern. At pH 1, the PL intensities have not increased when compared with pristine UiO-66-NH_2. At pH 2-3, the PL intensities surge noticeably. It can be attributed to the direct protonation of the amino group to form ammonium ion -NH_3^+ and the protonation of the anionic substrate species to form their corresponding molecules (H_2CO_3 and HF) at low pH. Consequently, the resultant protonated species cannot be held together. The gradual increase in PL intensity in CO_3^{2-} versus the sudden increase in F^- can be ascribed to the difference in pKa, where the pKa of HF (3.2) is notably lower than that of H_2CO_3 (pKa_1 = 6.4). Whereas, at increasing pH, the number of protonated amino groups reduces, which subsequently increases their interactions with the Lewis basic substrate ions.[45] We also noted reversible pH-dependent PL behavior, where the pH was first tuned to about 1 for 30 min before increasing the pH (see Figure S14). It suggests that the guest anions are retained at the adsorbed states during the pH adjustment. When the pH of the solution increases, we observed an apparent blueshift of the peak from 456 nm to 422 nm in both CO_3^{2-} and F^- substrates. The blueshift can be ascribed to the optoelectronic property of the parent UiO-66-NH_2 structure due to the deprotonation of the Zr_6O_4 nodes, where the pK_a values of the μ_3–OH, Zr–OH_2, and Zr–OH groups are 3.52, 6.79, and 8.30, respectively.[41] The electronic states of the nodes can directly affect the n→π^* ligand-to-cluster charge transfer behavior.

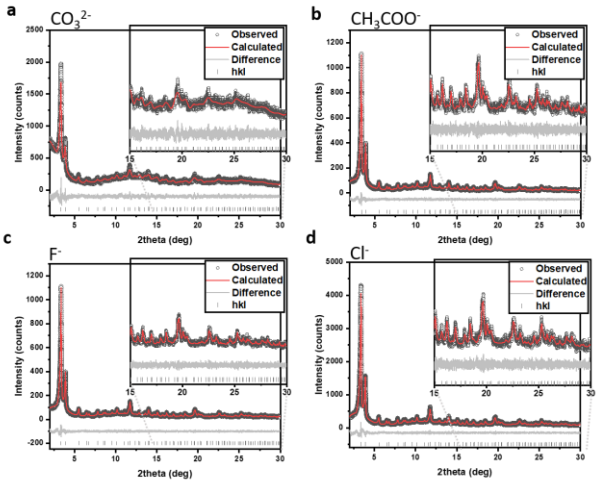

Figure 2. High-resolution PXRD patterns using Mo X-ray anode (λ = 0.7107 Å; E = 17.4 keV) and the corresponding Rietveld refinement profiles using TOPAS v6.0 of UiO-66-NH_2 loaded with (a) CO_3^{2-}, (b) CH_3COO^- (c) F^-, and (d) Cl^-. The crystallographic parameters are summarized in Table S1.

The influence of CO_3^{2-} and F^- on PL is believed to be beyond simply an electron charge transfer (from direct acid-base binding) as we do not note any alternation of PL upon adding CH_3COO^- and Cl^-. It implies that the presence of other critical factors, such as structural change. The structural chemistry of UiO-66-NH_2 has been well-studied, where the Zr_6O_4 nodal centers are coordinated with six ATA linkers in an octahedral arrangement. Herein, we employed a highly optimized capillary geometry using Mo anode as the X-ray source to study the structural information and atomic parameters. Fine powder samples were loaded in 0.5-mm borosilicate capillaries to reduce the packing issues with preferred orientation. An ultra-high angular resolution was achieved at 1 mdeg per step. The high-resolution PXRD patterns and the corresponding Rietveld refinement profiles of UiO-66-NH_2 loaded with different anions are shown in Figure 2. The crystal type remains cubic. The lattice parameters from Rietveld refinements are summarized in Table 1. Interestingly, the unit cell expands by 0.67% and 0.48% upon the addition of CO_3^{2-} and F^-, but contracts by 0.29% and 0.51% with CH_3COO^- and Cl^-. These structural findings coincide with our earlier observation that only the additions of CO_3^{2-} and F^- can noticeably enhance the PL intensities. Also, as the PL properties are pH-dependent, we have accordingly treated the samples with 0.5 M HCl or 0.5 M NaOH prior to PXRD measurements. The Bragg's peaks are less defined because of the interference with the solution (see Figures S15-S17). The crystal system remains at cubic with the space group of *Pnma*. Interestingly, the lattice parameters are found to be dependent on pH (see Table S2), with those at acidic conditions greater than those at basic conditions (between 1.0%-1.3%). There is only a slight difference between pristine UiO-66-NH_2 and those loaded with CO_3^{2-} and F^-. It suggests that although pH can notably affect the PL property, it only induces a slight structural change.

Table 1. Lattice parameters and cell volumes derived from Rietveld refinements of PXRD data of UiO-66-NH_2 samples loaded with different anions.

Sample	Crystal type; space group	Unit cell parameter a (Å)	Volume (Å^3)	Change in volume (%)
UiO-66-NH_2	Cubic; *Pnma*	20.78902(45)	8984.66(59)	N.A.
UiO-66-NH_2 + CO_3^{2-}	Cubic; *Pnma*	20.8354(18)	9044.91(24)	+0.67%
UiO-66-NH_2 + CH_3COO^-	Cubic; *Pnma*	20.76891(41)	8958.62(53)	0.29%
UiO-66-NH_2 + F^-	Cubic; *Pnma*	20.8221(65)	9027.68(84)	+0.48%
UiO-66-NH_2 + Cl^-	Cubic; *Pnma*	20.75337(55)	8938.53(72)	0.51%

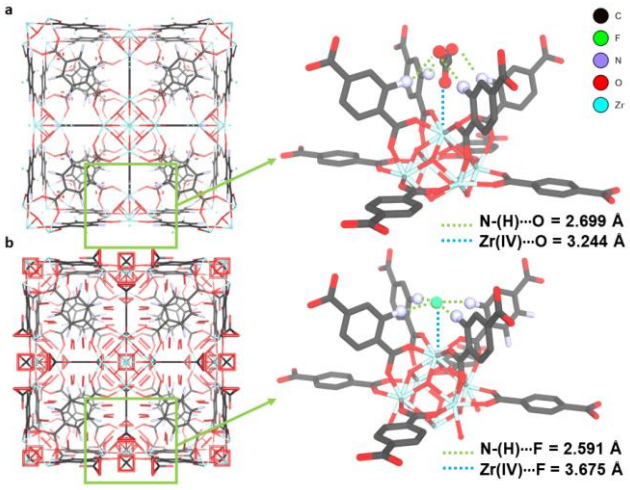

Figure 3. The refined crystal structures of UiO-66-NH_2 loaded with (a) CO_3^{2-}, and (b) F^-, from combined Rietveld refinement and density functional theory calculations. The corresponding refined crystal structures UiO-66-NH_2 loaded with CH_3COO^- and Cl^- are presented in Figure S19. Specific directions are selected to show the molecular pocket. The symmetry of the guest species is disregarded, and no hydrogens are plotted for clarity.

Given the high crystallinity of the UiO-66-NH_2 sample, the Rietveld refinements of high-resolution PXRD data can be applied to identify the atomic locations of the anionic sites. The derived crystal structures have been optimized using density functional theory calculations (see Figure 3 and the computational details in SI). The adsorbate interactions with respect to the host framework have been subsequently elucidated in terms of bond/molecular angles and distances. The Fourier maps showing the electron difference are shown in Figure S18; the atomic parameters are summarized in Tables S3-S6. As seen in the refined crystal structure of UiO-66-NH_2 loaded with CO_3^{2-}, the atomic location of the CO_3^{2-} species (Wyckoff letter of *24e*) is similar to that of F^- in UiO-66-NH_2. The interatomic distances between N_{linker} and O_{CO32-} are determined as 2.699(11) Å, in which each of the terminal O^- moieties of CO_3^{2-} species interacts with two neighboring linker amino groups. The interatomic angles are determined as $\angle O^-$-N-C = 103.8(15)°. By considering the hydrogen atom of the amine with the typical bond length of N-H of about 1.0 Å, the resultant H…O^- distance becomes about 1.7 Å, which falls in the range of medium hydrogen bonding.[46] The bridging coordination can be hereby understood as $(\text{-N(H)})_4\ldots CO_3^{2-}$. It should also be noted that the possible presence of the electrostatic stabilization of CO_3^{2-} by the Zr(IV) moiety at the nodal center where an interatomic distance of 3.244(9) Å was determined.

As seen in the refined crystal structures, the binding site of F^- is located between four neighboring linker amino groups, with the interatomic distances between N_{linker} and F^- of 2.591(8) Å (generated from mirror symmetry; Wyckoff letter of *24e*). The interatomic angles are determined as $\angle F^-$-N-C = 171.6(10)°. Similarly, the resultant H…F^- distances become about 1.6 Å[46], which suggests that the F^- also binds with the four neighboring amines with relatively strong hydrogen bonding interactions.[47] As this guest F^- species is located between four neighboring framework amine groups, a quaternary amine-fluoride ($(\text{-N(H)})_4\ldots F^-$) bridge is therefore formed at molecular distances. The hydrogen bonding can thus restrict the four neighboring ATA linkers from thermal rotation under thermodynamic equilibrium. On the other hand, the interatomic distance between F^- and Zr was determined as 3.675(15) Å, which suggests a weak electrostatic stabilization when compared with the case of CO_3^{2-}.

Evidently, the linkers are locked at this statistical orientation to achieve the most stable binding geometry with CO_3^{2-} and F^- under thermodynamic equilibrium. The four-fold symmetry operation of the space group of Fm-3m has facilitated the stabilization of the guest anions by the four surrounding amino groups of the UiO-66-NH_2 framework. Hence, it is evident that the formation of these hydrogen-bonded molecular bridges restricts the rotation of the linkers (as illustrated in Scheme 1), consequently enhancing the PL signals through the RRE effect.

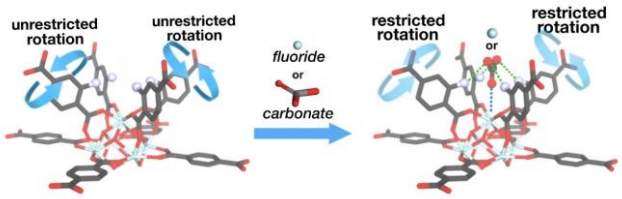

Scheme 1. Schematic illustration on the proposed mechanism of the restricted rotational freedom of C-C bond in the linker of UiO-66-NH_2 by the formation of quaternary hydrogen-bonded (-N(H))$_4$…X^- molecular bridge.

We have further investigated the crystal structures of UiO-66-NH_2 loaded with CH_3COO^- and Cl^- (see Figure S19). The site occupancy factor of Cl^- is low at 0.03(1), suggesting that UiO-66-NH_2 can only marginally adsorb Cl^- from the substrate. It is in agreement with the work by Lin *et al.* about the low uptake of Cl^- amongst a solution mixture of halides.[40] In the case of CH_3COO^-, the closest interatomic distance between the guest CH_3COO^- and the linker species is found at 2.71(2) Å. However, other interatomic distances are found at much longer values, suggesting the absence of a secondary bonding. As CH_3COO^- only possesses one formal negative charge, suggesting that it is unlikely to bridge the linker amino groups in the same manner as that of CO_3^{2-} in UiO-66-NH_2.

In general, the resonance structures of ATA offer thermodynamic stabilization to offer rotational rigidity along the axis of the C-C bond (see Figure S20). However, it is possible to perturb the rigidity of the linker species in some metal-modified UiO structures, by the incorporation of guest species, at the thermodynamic ground state.[26] We have therefore analyzed the rotational order by placing two rigid bodies Z-matrices, where matrix 1 describes the ATA linker with O and N atoms not on the same plane and matrix 2 with relaxed dihedral angles between O and N atoms. It is ultimately found that the site occupancy factor of matrix 2 tends to zero. This suggests that the coordination geometry remains at perfect octahedral at the nodal center. Therefore, the additional thermodynamic contribution from the coordination through hydrogen bonding with bridging F^- and CO_3^{2-} is insufficient to perturb the resonance stabilization from electron delocalization.

It has been noted that the PL increment for loading CO_3^{2-} on UiO-66-NH_2 is much higher than loading F- (*cf.* 1210% vs. 444%). When guest CO_3^{2-} and F^- ions adsorb on the UiO-66-NH_2, they not only affect the structural and atomic parameters as discussed above but also the electronic structures. As seen in Figure 4, our induced charge calculations show substantial changes in the electron densities between the guest anions and the framework -NH_2 groups, which are caused by the resultant hydrogen bonding interactions. The electron density increases much more significantly at the terminal O^- ends upon binding with CO_3^{2-} when compared with that of F^-, which can be correlated with the optical properties as discussed. Meanwhile, the electronic perturbation from the Zr-based nodal center is weak due to the relatively longer interatomic distances between the guest anions and the Zr atom (> 3.2 Å). It indicates that the hydrogen bonds play an important role in the adsorption behavior, which can further the RRE effect.

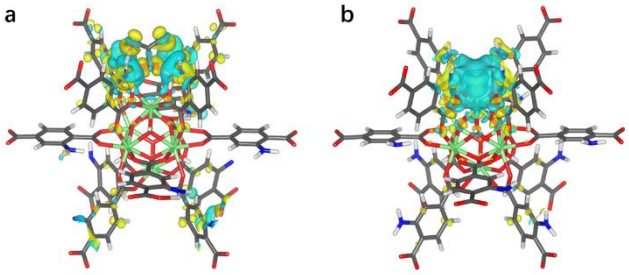

Figure 4. Induced charge rearrangement upon loading (a) CO_3^{2-} and (b) F^- on UiO-66-NH_2 at an iso-surface value of 2 × 10^{-4} e/Å^3. The blue zones indicate a decrease in electron density, whereas the yellow zones indicate an increase in electron density. Atoms are colored as follows: C (gray), N (blue), O (red), F (purple), Zr (green), and H (white). The experimental techniques can be found in the Methods section in SI.

Conclusions

In summary, this work has investigated the fundamental reasons for guest-anion-induced PL enhancement of UiO-66-NH_2 from the structural, electronic, and optical perspectives. Whereas the PL property in pristine UiO-66-NH_2 can be ascribed to n→π* charge transfer from the linker amino -NH_2 group to the Zr_6O_4 nodal center, the significantly enhanced PL signals can be attributed to the restricted rotation of the ATA linker *via* the formation of quaternary hydrogen-bonded (-N(H))$_4$…X^- molecular bridges, which subsequently perturbs the electronic structures. Akin to the chemistry of rotation-restricted emission as widely studied in related materials, the formation of these molecular bridges in UiO-66-NH_2 has hindered the rotational freedom of the single C-C bond in the ATA linkers. This work will shed light on the design of MOF-related materials for anion sensing and afford substantial progress in the fundamental reasoning of related luminescent materials.

Methods

Rietveld refinement of powder X-ray diffraction

High-solution powder X-ray diffraction data were collected at synchrotron beamline BL02B2 (energy = 18 keV; λ = 0.689556(2) Å), at SPring-8, Japan and in a highly optimized laboratory diffractometer equipped with Mo-anode X-ray tube (λ = 0.7107 Å). The samples were loaded in 0.5-mm borosilicate capillaries to reduce issues from sample textile and preferred orientation.

In total, there are more than 140 independent *hkl* reflections measured (within the region of refinement (2θ = 2-30°). From a mathematical perspective, the number of variables should not exceed the number of observables. In the Rietveld refinements performed in this work, the number of structural parameters has not exceeded 30. The lattice parameters were obtained using Pawley and Rietveld refinement methods. Analysis of the diffraction patterns was performed using the TOPAS v6.0 software. The background curve was fitted by a Chebyshev polynomial with an average of 12 coefficients. The Thompson-Cox-Hastings (pseudo-Voigt) function was applied to describe the diffraction peaks[32]. The scale factor and lattice parameters were allowed to vary for all the histograms.

The atomic locations of the framework atoms may change slightly – a small deviation from the starting model. Therefore, before the refinement of the entire structure with guest anions, the framework atoms and the positions of atoms were first refined. This was performed to avoid a miscalculation of the structure that reaches the global minimum of the refinement by changing the entire framework. Next, the Fourier analysis was used to identify the positions with the highest remaining electron density in the framework, once the positions of the host atoms have been determined.

Based on Fourier analysis, a Monte Carlo-based simulated annealing technique in which the guest anions as rigid bodies were used to locate their positions within the UiO-66-NH_2 framework. The rigid-body Z-matrices of the guest anions were refined while keeping the fractional coordinates of the framework atoms fixed. The relevant structural and atomic parameters were relaxed to be refined by simulated annealing repeatedly for an hour to ensure the global minimum has been reached. The global minimum is indicated by the lowest R_{wp} and *gof* values.

The B_{eq} were constrained in the following way: (i) all the framework Zr-sites share the same value as 0.6 $Å^2$, and the values for the framework O-sites as 2 $Å^2$, and (ii) the B_{eq} of the extra-framework atoms were all arbitrary fixed at 8 $Å^2$.[33–37] The position errors of the guest species were estimated from the percentage errors of the translation and rotation axes of the rigid bodies.

ASSOCIATED CONTENT

Supporting Information.
This material is available free of charge via the Internet at http://pubs.acs.org.
Details of material synthesis and calculation methods; physical characterization, including thermogravimetric analysis, surface area analysis, scanning electron microscopy, transmission electron microscopy; PL spectra in the solution with different pH levels; high-resolution powder XRD data and Rietveld refined crystal structure.

AUTHOR INFORMATION

Corresponding Author

*__Tsz Woon Benedict Lo__ - The Hong Kong Polytechnic University Shenzhen Research Institute, Shenzhen, China; State Key Laboratory of Chemical Biology and Drug Discovery, Department of Applied Biology and Chemical Technology, The Hong Kong Polytechnic University, Hong Kong, China; Email: benedict.tw.lo@polyu.edu.hk

Authors

†__Qi Xue__ - *The Hong Kong Polytechnic University Shenzhen Research Institute, Shenzhen, 519700, China; State Key Laboratory of Chemical Biology and Drug Discovery, Department of Applied Biology and Chemical Technology, The Hong Kong Polytechnic University, Hong Kong, China*

†__Ka Hin Chan__ - The Hong Kong Polytechnic University Shenzhen Research Institute, Shenzhen, China; State Key Laboratory of Chemical Biology and Drug Discovery, Department of Applied Biology and Chemical Technology, The Hong Kong Polytechnic University, Hong Kong, China

__Cheuk Ki Yim__ - *State Key Laboratory of Chemical Biology and Drug Discovery, Department of Applied Biology and Chemical Technology, The Hong Kong Polytechnic University, Hong Kong, China*

__Bryan Kit Yue Ng__ - *Department of Chemistry, University of Oxford, Oxford, OX1 3QR, United Kingdom*

__Tianxiang Chen__ - *State Key Laboratory of Chemical Biology and Drug Discovery, Department of Applied Biology and Chemical Technology, The Hong Kong Polytechnic University, Hong Kong, China*

__Sarah Day__ - *Diamond Light Source, Harwell Campus, Didcot, OX11 0DE, United Kingdom*

__Chiu Chung Tang__ - *Diamond Light Source, Harwell Campus, Didcot, OX11 0DE, United Kingdom*

__Shogo Kawaguchi__ - *SPring-8, Hyogo, 679-5198, Japan*

__Kwok-Yin Wong__ - *State Key Laboratory of Chemical Biology and Drug Discovery, Department of Applied Biology and Chemical Technology, The Hong Kong Polytechnic University, Hong Kong, China*

Author Contributions

The manuscript was written through the contributions of all authors. QX, KHC, and CKY were responsible for the main part of the experiments. BKYN, TC, SD, CCT and SW offered help in structural characterization. K-YW provided general advice. TWBL was responsible for the entire project. All authors have approved the final version of the manuscript.
†These authors contributed equally.

Notes

The authors declare no competing financial interest.

ACKNOWLEDGMENT

This work was supported by the National Natural Science Foundation of China (21902139) and the Hong Kong Research Grants Council (25300918 and 15300819) for financial support (TWBL). We thank SPring-8 (2018B1081), and UMF, UCEA and ULS of HKPU for the support in material characterization.

REFERENCES

(1) Medishetty, R.; Zaręba, J. K.; Mayer, D.; Samoć, M.; Fischer, R. A. Nonlinear Optical Properties, Upconversion and Lasing in Metal–Organic Frameworks. *Chem. Soc. Rev.* **2017**, *46* (16), 4976–5004.

(2) Stavila, V.; Talin, A. A.; Allendorf, M. D. MOF-Based Electronic and Opto-Electronic Devices. *Chem. Soc. Rev.* **2014**, *43* (16), 5994–6010.

(3) Shen, X.; Yan, B. Polymer Hybrid Thin Films Based on Rare Earth Ion-Functionalized MOF: Photoluminescence Tuning and Sensing as a Thermometer. *Dalt. Trans.* **2015**, *44* (4), 1875–1881.

(4) Yang, L.; Choi, C.; Hong, S.; Liu, Z. Single Yttrium Sites on Carbon-Coated TiO2 for Efficient Electrocatalytic N2 Reduction. *Chem. Commun.* **2020**, *56*, 10910–10913.

(5) Luo, F.; Batten, S. R. Metal–Organic Framework (MOF): Lanthanide (III)-Doped Approach for Luminescence Modulation and Luminescent Sensing. *Dalt. Trans.* **2010**, *39* (19), 4485–4488.

(6) Wei, J.-Z.; Gong, F.-X.; Sun, X.-J.; Li, Y.; Zhang, T.; Zhao, X.-J.; Zhang, F.-M. Rapid and Low-Cost Electrochemical Synthesis of UiO-66-NH2 with Enhanced Fluorescence Detection Performance. *Inorg. Chem.* **2019**, *58* (10), 6742–6747.

(7) Zhu, H.; Huang, J.; Zhou, Q.; Lv, Z.; Li, C.; Hu, G. Enhanced Luminescence of NH2-UiO-66 for Selectively Sensing Fluoride Anion in Water Medium. *J. Lumin.* **2019**, *208*, 67–74.

(8) Ma, D.; Li, B.; Zhou, X.; Zhou, Q.; Liu, K.; Zeng, G.; Li,

G.; Shi, Z.; Feng, S. A Dual Functional MOF as a Luminescent Sensor for Quantitatively Detecting the Concentration of Nitrobenzene and Temperature. *Chem. Commun.* **2013**, *49* (79), 8964–8966.

(9) Müller-Buschbaum, K.; Beuerle, F.; Feldmann, C. MOF Based Luminescence Tuning and Chemical/Physical Sensing. *Microporous Mesoporous Mater.* **2015**, *216*, 171–199.

(10) Hu, Z.; Deibert, B. J.; Li, J. Luminescent Metal–Organic Frameworks for Chemical Sensing and Explosive Detection. *Chem. Soc. Rev.* **2014**, *43* (16), 5815–5840.

(11) Allendorf, M. D.; Bauer, C. A.; Bhakta, R. K.; Houk, R. J. T. Luminescent Metal–Organic Frameworks. *Chem. Soc. Rev.* **2009**, *38* (5), 1330–1352.

(12) Jensen, S.; Tan, K.; Lustig, W. P.; Kilin, D. S.; Li, J.; Chabal, Y. J.; Thonhauser, T. Structure-Driven Photoluminescence Enhancement in a Zn-Based Metal–Organic Framework. *Chem. Mater.* **2019**, *31* (19), 7933–7940.

(13) Feng, P. L.; Leong, K.; Allendorf, M. D. Charge-Transfer Guest Interactions in Luminescent MOFs: Implications for Solid-State Temperature and Environmental Sensing. *Dalt. Trans.* **2012**, *41* (29), 8869–8877.

(14) Sussardi, A.; Hobday, C. L.; Marshall, R. J.; Forgan, R. S.; Jones, A. C.; Moggach, S. A. Correlating Pressure-induced Emission Modulation with Linker Rotation in a Photoluminescent MOF. *Angew. Chem. Int. Ed.,* **2020**, *132* (21), 8195–8199.

(15) Senkovska, I.; Hoffmann, F.; Fröba, M.; Getzschmann, J.; Böhlmann, W.; Kaskel, S. New Highly Porous Aluminium Based Metal-Organic Frameworks: Al (OH)(Ndc)(Ndc= 2, 6-Naphthalene Dicarboxylate) and Al (OH)(Bpdc)(Bpdc= 4, 4′-Biphenyl Dicarboxylate). *Microporous mesoporous Mater.* **2009**, *122* (1–3), 93–98.

(16) Yoskamtorn, T.; Zhao, P.; Wu, X.-P.; Purchase, K.; Orlandi, F.; Manuel, P.; Taylor, J.; Li, Y.; Day, S.; Ye, L. Responses of Defect-Rich Zr-Based Metal–Organic Frameworks toward NH3 Adsorption. *J. Am. Chem. Soc.* **2021**, *143* (8), 3205–3218.

(17) Yin, H.-Q.; Wang, X.-Y.; Yin, X.-B. Rotation Restricted Emission and Antenna Effect in Single Metal–Organic Frameworks. *J. Am. Chem. Soc.* **2019**, *141* (38), 15166–15173.

(18) Benson, O.; Da Silva, I.; Argent, S. P.; Cabot, R.; Savage, M.; Godfrey, H. G. W.; Yan, Y.; Parker, S. F.; Manuel, P.; Lennox, M. J. Amides Do Not Always Work: Observation of Guest Binding in an Amide-Functionalized Porous Metal–Organic Framework. *J. Am. Chem. Soc.* **2016**, *138* (45), 14828–14831.

(19) Bordiga, S.; Lamberti, C.; Ricchiardi, G.; Regli, L.; Bonino, F.; Damin, A.; Lillerud, K.-P.; Bjorgen, M.; Zecchina, A. Electronic and Vibrational Properties of a MOF-5 Metal–Organic Framework: ZnO Quantum Dot Behaviour. *Chem. Commun.* **2004**, No. 20, 2300–2301.

(20) Lustig, W. P.; Mukherjee, S.; Rudd, N. D.; Desai, A. V; Li, J.; Ghosh, S. K. Metal–Organic Frameworks: Functional Luminescent and Photonic Materials for Sensing Applications. *Chem. Soc. Rev.* **2017**, *46* (11), 3242–3285.

(21) Lin, R.; Liu, S.; Ye, J.; Li, X.; Zhang, J. Photoluminescent Metal–Organic Frameworks for Gas Sensing. *Adv. Sci.* **2016**, *3* (7), 1500434.

(22) Kreno, L. E.; Leong, K.; Farha, O. K.; Allendorf, M.; Van Duyne, R. P.; Hupp, J. T. Metal–Organic Framework Materials as Chemical Sensors. *Chem. Rev.* **2012**, *112* (2), 1105–1125.

(23) Hu, Z.; Tan, K.; Lustig, W. P.; Wang, H.; Zhao, Y.; Zheng, C.; Banerjee, D.; Emge, T. J.; Chabal, Y. J.; Li, J. Effective Sensing of RDX via Instant and Selective Detection of Ketone Vapors. *Chem. Sci.* **2014**, *5* (12), 4873–4877.

(24) Pramanik, S.; Zheng, C.; Zhang, X.; Emge, T. J.; Li, J. New Microporous Metal− Organic Framework Demonstrating Unique Selectivity for Detection of High Explosives and Aromatic Compounds. *J. Am. Chem. Soc.* **2011**, *133* (12), 4153–4155.

(25) Hu, R.; Leung, N. L. C.; Tang, B. Z. AIE Macromolecules: Syntheses, Structures and Functionalities. *Chem. Soc. Rev.* **2014**, *43* (13), 4494–4562.

(26) Wong, Y.-L.; Diao, Y.; He, J.; Zeller, M.; Xu, Z. A Thiol-Functionalized UiO-67-Type Porous Single Crystal: Filling in the Synthetic Gap. *Inorg. Chem.* **2018**, *58* (2), 1462–1468.

(27) Yee, K.-K.; Reimer, N.; Liu, J.; Cheng, S.-Y.; Yiu, S.-M.; Weber, J.; Stock, N.; Xu, Z. Effective Mercury Sorption by Thiol-Laced Metal–Organic Frameworks: In Strong Acid and the Vapor Phase. *J. Am. Chem. Soc.* **2013**, *135* (21), 7795–7798.

(28) Cejka, J.; Corma, A.; Zones, S. *Zeolites and Catalysis: Synthesis, Reactions and Applications*; John Wiley & Sons, 2010.

(29) Chen, T.; Huang, B.; Day, S.; Tang, C. C.; Tsang, S. C. E.; Wong, K. Y.; Lo, B. T. W. Differential Adsorption of L- and d-Lysine on Achiral MFI Zeolites as Determined by Synchrotron X-Ray Powder Diffraction and Thermogravimetric Analysis. *Angew. Chem. Int. Ed.* **2020**, *59* (3), 1093–1097.

(30) Lo, B. T. W.; Ye, L.; Tsang, S. C. E. The Contribution of Synchrotron X-Ray Powder Diffraction to Modern Zeolite Applications: A Mini-Review and Prospects. *Chem* **2018**, *4* (9), 1–31.

(31) Yang, S.; Sun, J.; Ramirez-Cuesta, A. J.; Callear, S. K.; David, W. I. F.; Anderson, D. P.; Newby, R.; Blake, A. J.; Parker, J. E.; Tang, C. C.; Schröder, M. Selectivity and Direct Visualization of Carbon Dioxide and Sulfur Dioxide in a Decorated Porous Host. *Nat. Chem.* **2012**, *4* (11), 887–894.

(32) Thompson, P.; Cox, D. E.; Hastings, J. B. Rietveld Refinement of Debye-Scherrer Synchrotron X-Ray Data from Al2O3. *J. Appl. Crystallogr.* **1987**, *20* (2), 79–83.

(33) Watkin, D. Uequiv: Its Past, Present and Future. *Acta Crystallogr. Sect. B Struct. Sci.* **2000**, *56* (5), 747–749.

(34) Cooper, R. I.; Thompson, A. L.; Watkin, D. J. CRYSTALS Enhancements: Dealing with Hydrogen Atoms in Refinement. *J. Appl. Crystallogr.* **2010**, *43* (5 PART 1), 1100–1107.

(35) Van Koningsveld, H. High-Temperature (350 K) Orthorhombic Framework Structure of Zeolite H-ZSM-5. *Acta Crystallogr. Sect. B Struct. Sci.* **1990**, *46* (6), 731–735.

(36) Mentzen, B. F. Characterization of Guest Molecules Adsorbed on Zeolites of Known Structure by Combined X-Ray Powder Profile Refinements and Conventional Difference-Fourier Techniques. Part II-Localization of the n-Hexane, TPA and p-Xylene Guests in a Pentasil Type Zeoli. *Mater. Res. Bull.* **1987**, *22* (4), 489–496.

(37) Goyal, R.; Fitch, A. N.; Jobic, H. Powder Neutron and X-Ray Diffraction Studies of Benzene Adsorbed in Zeolite ZSM-5. *J. Phys. Chem. B* **2000**, *104* (13), 2878–2884.

(38) Valenzano, L.; Civalleri, B.; Chavan, S.; Bordiga, S.; Nilsen, M. H.; Jakobsen, S.; Lillerud, K. P.; Lamberti, C. Disclosing the Complex Structure of UiO-66 Metal

Organic Framework: A Synergic Combination of Experiment and Theory. *Chem. Mater.* **2011**, *23* (7), 1700–1718.

(39) Sun, C.; Wang, X.; Qin, C.; Jin, J.; Su, Z.; Huang, P.; Shao, K. Solvatochromic Behavior of Chiral Mesoporous Metal–Organic Frameworks and Their Applications for Sensing Small Molecules and Separating Cationic Dyes. *Chem. Eur. J.* **2013**, *19* (11), 3639–3645.

(40) Lin, K.-Y. A.; Liu, Y.-T.; Chen, S.-Y. Adsorption of Fluoride to UiO-66-NH2 in Water: Stability, Kinetic, Isotherm and Thermodynamic Studies. *J. Colloid Interface Sci.* **2016**, *461*, 79–87.

(41) Li, X.; Zhang, H.; Wang, P.; Hou, J.; Lu, J.; Easton, C. D.; Zhang, X.; Hill, M. R.; Thornton, A. W.; Liu, J. Z.; Freeman, B. D.; Hill, A. J.; Jiang, L.; Wang, H. Fast and Selective Fluoride Ion Conduction in Sub-1-Nanometer Metal-Organic Framework Channels. *Nat. Commun.* **2019**, *10* (1), 1–12.

(42) Shrivastava, A.; Gupta, V. B. Methods for the Determination of Limit of Detection and Limit of Quantitation of the Analytical Methods. *Chronicles young Sci.* **2011**, *2* (1), 21.

(43) Fawell, J.; Bailey, K.; Chilton, J.; Dahi, E.; Magara, Y. *Fluoride in Drinking-Water*; IWA publishing, 2006.

(44) Xue, Q.; Xie, Y.; Wu, S.; Wu, T. S.; Soo, Y. L.; Day, S.; Tang, C. C.; Man, H. W.; Yuen, S. T.; Wong, K. Y.; Wang, Y.; Lo, B. T. W.; Tsang, S. C. E. A Rational Study on the Geometric and Electronic Properties of Single-Atom Catalysts for Enhanced Catalytic Performance. *Nanoscale* **2020**, *12* (45), 23206–23212.

(45) Pan, D.; Zhang, J.; Li, Z.; Wu, C.; Yan, X.; Wu, M. Observation of PH-, Solvent-, Spin-, and Excitation-Dependent Blue Photoluminescence from Carbon Nanoparticles. *Chem. Commun.* **2010**, *46* (21), 3681–3683.

(46) Tarakanova, E. G.; Yukhnevich, G. V. Relationship between the Bond Lengths in NH... N, OH... O, FH... F, and Cl-H... Cl Hydrogen Bridges. *J. Struct. Chem.* **2009**, *50* (6), 1015–1020.

(47) Ye, L.; Lo, B. T. W.; Qu, J.; Wilkinson, I.; Hughes, T.; Murray, C. A.; Tang, C. C.; Tsang, S. C. E. Probing Atomic Positions of Adsorbed Ammonia Molecules in Zeolite. *Chem. Commun.* **2016**, *52* (16), 3422–3425.

Table of Contents artwork